Spectroscopic ellipsometric properties and resistance switching behavior in $Si_x(ZrO_2)_{100-x}$ films

Xiaodong Wang (王骁栋)[1], Liang Feng (冯 亮)[1], Shenjin Wei (魏慎金)[1], Huanfeng Zhu (朱焕锋)[1], Kun Chen (陈 坤)[1], Da Xu (徐 达)[1], Ying Zhang(张 颖)[1], and Jing Li (李 晶)[1,2*]

[1]*Department of Optical Science and Engineering, Fudan University, Shanghai 200433, China*

[2]*Key Laboratory of Micro and Nano Photonic Structures (Ministry of Education), Fudan University, Shanghai 200433, China*

[*]*Corresponding author: lijing@fudan.edu.cn*

Received November 17, 2010; accepted December 17, 2010; posted online April 18, 2011

We prepare $Si_x(ZrO_2)_{100-x}$ composite films using the co-sputtering method. The chemical structures of the films which are prepared under different conditions are analyzed with X-ray photoemission spectroscopy. Thermal treatment influences on optical property and resistance switching characteristics of these composite films are investigated by spectroscopic ellipsometry and semiconductor parameter analyzer, respectively. With the proper Si-doped $Si_x(ZrO_2)_{100-x}$ interlayer, the Al/ $Si_x(ZrO_2)_{100-x}$/Al device cell samples present very reliable and reproducible switching behaviors. It provides a feasible solution for easy multilevel storage and better fault tolerance in nonvolatile memory application.

OCIS codes: 310.6188, 310.6860, 250.6715.

doi: 10.3788/COL201109.053102.

Next generation nonvolatile memory has attracted extensive attention as traditional memories approach their scaling limits[1]. A promising candidate is the resistance random access memory (RRAM) due to its superior characteristics, including simple structure, high density integration, low power consumption, and high write/erase rate[2]. Current candidate materials for RRAM devices include ferromagnetic material, organic material, doped perovskite, and binary oxides such as NiO, TiO_2, Al_2O_3, and Cu_xO[3−7]. Lee *et al.* reported the resistance switching behavior of non-stoichiometric zirconium oxide (ZrO_x)[8]. Our previous study found a resistance switching effect in stoichiometric ZrO_2 film and provided a feasible way to improve device yield by using it instead of non-stoichiometric ZrO_x film[9]. Guan *et al.* indicated that intentionally introduced external traps in ZrO_2 films could significantly improve device yield due to more uniform and homogeneous trap concentrations[10]. Influences on the optical properties of Y_2O_3-doped ZrO_2 thin films have been reported[11]. Metal nanoparticles such as Au, Ag, and Cu doped into ZrO_2 films have been confirmed to improve resistance switching characteristics[12−14]. However, Si dopant may play an important role in improving resistance switching behavior in Si-doped ZrO_2 films.

In this letter, $Si_x(ZrO_2)_{100-x}$ (SZO) composite films were prepared using the co-sputtering method. The chemical structures, spectroscopic properties, and resistance switching characteristics under different conditions were analyzed by X-ray photoemission spectroscopy (XPS), spectroscopic ellipsometry (SE), and semiconductor parameter analyzer (SPA), respectively.

The SZO composite films were prepared using the LAB600sp multi-target magnetron sputtering system with co-sputtering method. To obtain suitable content of Si dopant in the ZrO_2 matrix, the ZrO_2 (99.99%) targets were mounted at a fixed angle of 45° relative to the normal plane of a Si(100) substrate on the object stage. The other Si (99.99%) targets were mounted at 30°, 35°, and 45° relative to that of the same substrates, respectively. Sputtering powers were kept constant for both ZrO_2 and Si targets. Four groups of as-deposition samples, named sample A, B, C, and D, were prepared. The specific preparation parameters are shown in Table 1.

To analyze the thermal stability of these samples, thermal treatments were carried out at annealing temperatures of 200 and 300 °C with an annealing time of 15 min, respectively. The chemical structures of the sample films were analyzed by XPS. The optical properties of the sample films were measured using the SE method in the photon energy range from 1.5 to 4.5 eV at three different incidence angles of 65°, 70°, and 75°, respectively. All optical constants of the samples were obtained after fitting using the commercial software Film Wizard®.

A series of Al/$Si_x(ZrO_2)_{100-x}$/Al (ASZOA) multilayer samples as device cells was fabricated for the sake of investigating resistance switching behaviors. After thermal oxidation of a 2-inch-diameter Si(100) substrate wafer, an Al layer was deposited as bottom electrode by direct current (DC) magnetron sputtering. Then, a SZO film with a gradually changed composition was deposited on the Al/SiO_2/Si substrate wafer by co-sputtering method with a self-designed auxiliary baffle. Finally, Al top-electrode lattice points with a diameter of 100 μm were deposited by DC magnetron sputtering through a shadow mask. The working vacuum was 8.0×10^{-3} mbar for the

Table 1. Preparation Parameters of the SZO Films

Sample No.	A	B	C	D
Sputtering Powers (W)/ Angles for Si (deg.)	0/−−	20/30	20/35	20/45
Sputtering Powers (W)/ Angles for ZrO_2 (deg.)	200/45	200/45	200/45	200/45
Sputtering Time (s)	1200	1200	1200	1200
Working Vacuum (10^{-3} mbar)	8	8	8	8

 © 2011 Chinese Optics Letters

entire sputtering process. The chemical bonding states of Zr, Si, and O elements, and Si concentration percentages in the SZO composite films were determined by XPS analyses. Resistance switching characteristics of the ASZOA samples were measured by a Keithley 4200-SCS SPA.

Measurements were performed on the SZO and ASZOA samples using the aforementioned methods. The XPS spectra, SE properties of SZO, and resistance switching characteristics of ASZOA are given as follows.

According to XPS measurements, the mole percentages of Si dopant in the SZO film samples B, C, and D are 2.6%, 4.9%, and 8.4%, respectively. The XPS spectra of Zr, Si, and O elements in the SZO film samples B, C, and D are shown in Fig. 1.

With the increase of Si dopant, there is an obvious transformation of the chemical states of those elements. All the Zr $3d_{5/2}$, Zr $3d_{3/2}$, and Si 2p peaks shift toward the high energy region, but the O 1s peaks move over to the left. In Fig. 1(a), the Zr $3d_{5/2}$ and Zr $3d_{3/2}$ peaks of sample B have binding energies of 182.0 and 184.4 eV, respectively. The energy interval of 2.4 eV between the two peaks indicates the Zr element is in the fully oxidized value of Zr^{4+}. Corresponding to sample C, the energy interval between the Zr $3d_{5/2}$ and Zr $3d_{3/2}$ peaks keeps the same value, although the two peaks shift a little toward the high energy region. While the percentage of Si dopant increased to 8.4% (sample D), the two Zr peaks changed distinctly and the energy interval decreased to about 2.1 eV. This indicates that not all the chemical values of Zr are Zr^{4+} in this case. The same situation occurred in Si 2p and O 1s spectra according to Figs. 1(b) and (c). Obviously, a fraction of Zr-O chemical bonds were transformed into Si-O chemical bonds with the increase of Si concentrations.

The optical properties of the SZO films can be obtained in detail by means of SE measurement. In SE measurement, the two ellipsometric parameters ψ, Δ are related to the optical and structural properties of materials. It is defined by

$$\rho = r_{\mathrm{p}}/r_{\mathrm{s}} = \tan\psi \exp(\mathrm{i}\Delta), \quad (1)$$

where r_{p} and r_{s} are the complex reflective coefficients of parallel and perpendicular polarized light to the incidence plane, respectively. The ellipsometric spectra of ψ, Δ of SZO films in the energy range of 1.5–4.5 eV are shown in Figs. 2(a) and (b), respectively.

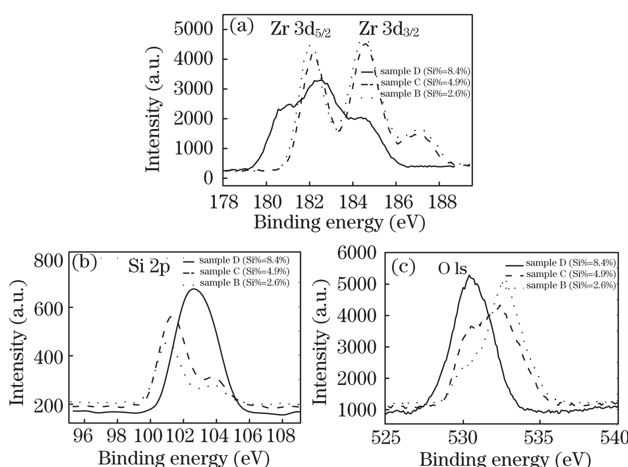

Fig. 1. XPS spectra of (a) Zr 3d, (b) Si 2p, and (c) O 1s for the SZO samples B, C, and D, respectively.

The SE spectra can be analyzed by a simple three-phase model consisting of Si substrate/SZO film/ambient (n=1). In this model, unknown parameters of the film thickness d_{f} and dielectric constant ε for the SZO films are designated as fitting variables. The Lorentz oscillator model (LOM) is adopted to calculate the dielectric functions of the SZO films described as

$$\varepsilon = \varepsilon_1 + \mathrm{i}\varepsilon_2 = \varepsilon_\infty \left(1 + \sum_i \frac{A_i^2}{C_i^2 - E^2 - \mathrm{j}\nu_i E}\right), \quad (2)$$

where ε_∞ is the dielectric constant of optical frequency; A_i, C_i, and v_i are the amplitude, central energy, and damping coefficient of each oscillator, respectively. The A_i value also represents the percentage contribution of oscillator i in the whole system. The complex refractive index can be calculated from the dielectric function using

$$n = \left[\frac{1}{2}\sqrt{\varepsilon_1^2 + \varepsilon_2^2} + \varepsilon_1\right]^{1/2}, k = \left[\frac{1}{2}\sqrt{\varepsilon_1^2 + \varepsilon_2^2} - \varepsilon_1\right]^{1/2}. \quad (3)$$

According to the SE spectra above, the refractive index n and extinction coefficient k can be calculated in Fig. 3.

With the concentration augment of Si dopant, both n and k curves of the SZO films B, C, and D increase in whole. The n curve of sample D is less than that of the pure ZrO_2 film in the high energy range of 3.4–4.5 eV, but it is larger in the low energy range of 1.5–3.4 eV. These results can be explained by concentrations of the Si dopant influence on the chemical structure of the composite films.

To analyze thermal stability of the SZO films, thermal treatments were carried out to samples B, C, and D. After annealing, the optical constants of these samples were measured by SE. Figures 4–6 illustrate the n and k curves of sample B, C, and D at different annealing

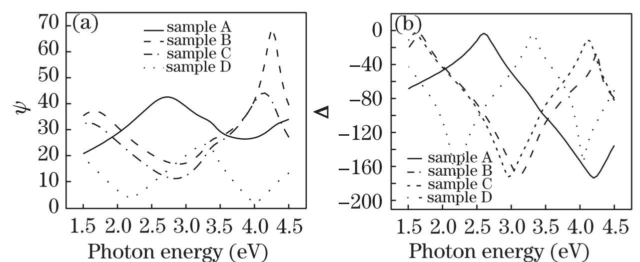

Fig. 2. (a) ψ and (b) Δ spectra of SZO film samples with different concentrations.

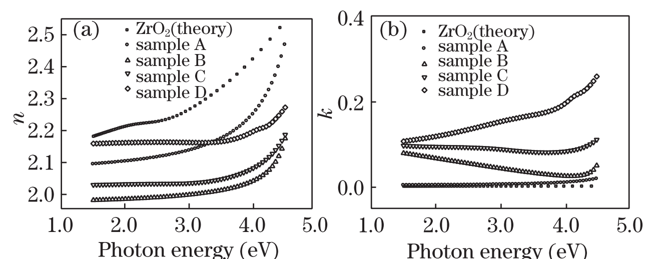

Fig. 3. (a) n and (b) k curves of SZO films.

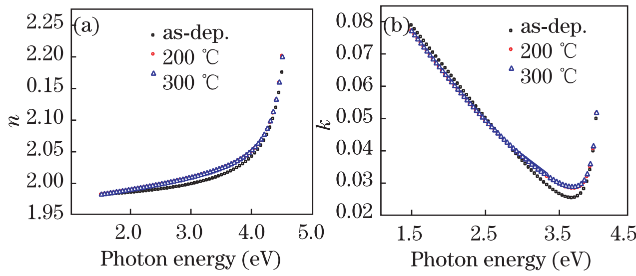

Fig. 4. (a) n and (b) k curves of sample B at different annealing temperatures.

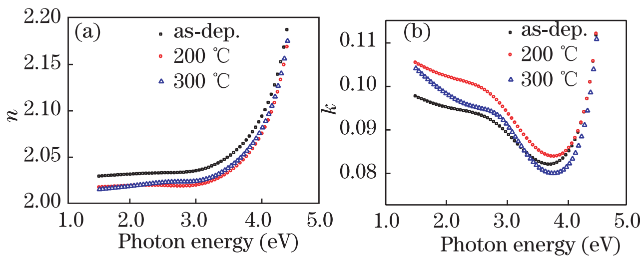

Fig. 5. (a) n and (b) k curves of sample C at different annealing temperatures.

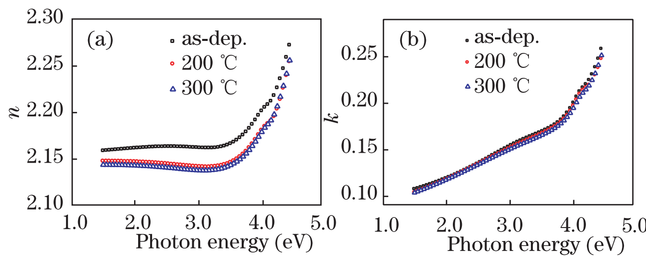

Fig. 6. (a) n and (b) k curves of sample D at different annealing temperatures.

temperatures, respectively.

All the optical constants n and k curves show the same variation trend clearly after annealing at 200 °C and 300 °C, respectively. A comparison of those curves in samples B, C, and D indicates that the deviation of optical constants increase gradually with the concentration rise of Si dopant after annealing. The XPS measurements had already demonstrated that Zr^{4+} was not the only chemical value in the SZO films with the higher concentration of Si dopant. It was also possible that Zr-O and Si-O or Zr-O-Si chemical bonds existed. The favorable composite films have sufficiently good thermal stability below the testing temperatures.

The ASZOA device cells, named sample Nos. 1 to 6, were prepared by SPA to measure their resistance switching behaviors. After XPS analyses, the Si doping concentrations in each SZO interlayer of sample Nos. 1 to 6 were 2.6%, 2.9%, 3.3%, 3.8%, 4.3%, and 4.9%, respectively. Figure 7 shows one group of testing results for the typical electric current-voltage *(I-V)* characteristics of these RRAM sample cells Nos. 1 to 6.

According to the I-V characteristic curves, these samples clearly show a unipolar switching behavior. After the initial forming process at a certain voltage between 8.0 and 10.0 V, one of the samples reached a low resistance state (LRS), which is usually called on-state. By sweeping the applied positive voltage to a certain value between 0.6 and 1.8 V with a clamping current of 0.1 A, a sudden drop of current appeared and one of the samples returned to a high resistance state (HRS), which is so-called off-state. A higher sweeping voltage of 3.8–7.8 V to be kept on with a lower clamping current of 0.02 A, an abrupt increase of the current appeared and the on state attained.

After logarithmic transformations of the I-V testing data in the low voltage region ($V < V_{\rm reset}$), the ln$I$ versus ln$V$ curves of the samples were obtained (see Fig. 8).

According to Ohm's Law, $V = IR$. The slope of ln$I$ versus ln$V$ curve is equal to 1 after logarithmic transformation of I-V data. In Fig. 8, both the slopes of LRS and HRS curves are approximately equal to 1. In addition, the fitting slope values of ln$I$/ln$V$ for samples Nos. 1 to 6 with different Si doping concentrations are shown in Fig. 9. It indicates that these sample cells present ohmic behavior in the low voltage region.

It is natural to suggest that the ASZOA structure has a Schottky nature because the Schottky equation is widely used in the leakage current analysis of the metal/semiconductor structure. The I-V relation can be expressed as

$$I \propto T^2 \exp\left(\frac{e\sqrt{(eV)/(4\pi\varepsilon_{\rm i}\varepsilon_0 d)}}{kT}\right), \tag{4}$$

where I is the current, e is the electronic charge, ε_0 is the permittivity in vacuum, $\varepsilon_{\rm i}$ is the optical dielectric constant, V is the applied voltage, d is the thickness of a film, k is the Boltzmann's constant, and T is temperature. If the Schottky conduction is obeyed in HRS, a linear relationship between ln$I$ versus $V^{1/2}$ should be obtained in the following equation

$$\ln I \propto \ln T^2 + \frac{e\sqrt{e/(4\pi\varepsilon_{\rm i}\varepsilon_0 d)}}{kT}V^{1/2}. \tag{5}$$

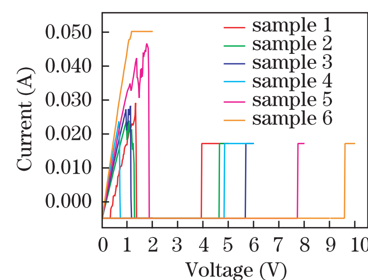

Fig. 7. (Color online) One group of I-V characteristics of the RRAM sample cells Nos. 1 to 6.

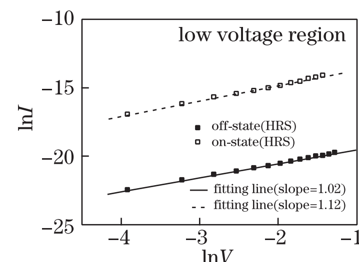

Fig. 8. ln$I$ versus ln$V$ curves of the samples in low voltage region.

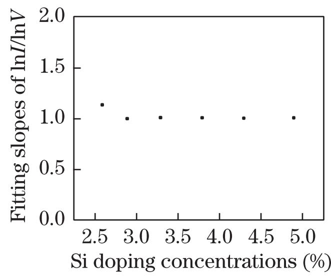

Fig. 9. Fitting slopes of ln$I$ versus ln$V$ curves of the samples in low voltage region.

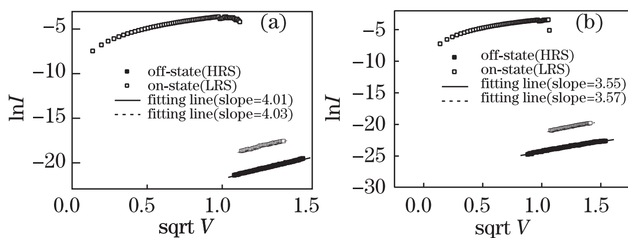

Fig. 10. ln$I$ versus $V^{1/2}$ curves of the No. (a) 2 and (b) 3 cells in high voltage region.

The diagrams of the ln$I$ versus $V^{1/2}$ curves of Nos. 2 and 3 cells are shown in Fig. 10. It can be found that the ln$I$ versus $V^{1/2}$ curves present a linear relation between both Nos. 2 and 3 cells in the high voltage region.

According to the following formula

$$\text{slope} = \frac{e\sqrt{e/(4\pi\varepsilon_i\varepsilon_0 d)}}{kT}, \quad (6)$$

the ε_i-slope relation can be expressed as

$$\varepsilon_i \propto 1/\text{slope}^2. \quad (7)$$

In comparison to the slopes in Figs. 10(a) and (b), the slopes obviously decrease with the increase of Si dopant concentration and the ε_i increase with the decrease of slope. The increase of ε_i predicts that the resistance of SZO will rise up in HRS. It is advantageous to improve the on/off ratio.

A whole resistance switching cycle includes two processes: one from the HRS to LRS process to be called "set", the other is from the LRS to HRS process and goes by the name of "reset". After a multitude of tests, the reliable switching cycles were obtained in the Nos. 1 to 5 cells. It was not successful to switch back to HRS from LRS in the No. 6 cell.

Obviously, the greater the increase in Si-doped concentration of the SZO interlayer, the higher the set voltage (V_{set}) rises. Moreover, the resistance of HRS reached 5×10^9 kΩ while the resistance of LRS was 40 Ω in the test. The on/off ratio between HRS and LRS is larger than 10^8, which is also much larger than that of the Al/ZrO_2/Al device[9]. Therefore, the giant on/off ratio certainly suggests a possibility to achieve high density memory by means of multibit or multilevel storage, and better fault tolerance in future applications.

In conclusion, a series of SZO films and ASZOA cells is prepared. Their optical constants are mainly influenced by the concentration of the Si dopant, and the physical and chemical structure of the SZO films. All the optical constants show the same variation trend after annealing. Experimental results show that the favorable composite films have sufficiently good thermal stability below the testing temperatures. With the proper Si-doped SZO interlayer, the ASZOA device samples present very reliable and reproducible switching behaviors. The V_{set} voltage of the sample cells increases with the augment of Si concentration. The on/off ratio between two stable states is as large as 10^8, which is also much larger than that of the Al/ZrO_2/Al device. It provides a possible solution for easy multilevel storage and better fault tolerance of nonvolatile memory.

This work was supported by the National Nature Science Foundation of China (No. 60578047), and the National "973" Program of China (Nos. 2009CB929201 and No.2010CB933703). The authors would like to thank the assistance of Prof. T. X. Liu in the XPS test and Prof. P. Zhou in the SPA tests.

References

1. A. Allen, "International Technology Roadmap For Semiconductors: Some Overview Highlights", http://masttech.com.tw/itrs_jan08.pdf (2007).
2. R. Waser, R. Dittmann, G. Staikov, and K. Szot, Adv. Mate. **21,** 2632 (2009).
3. S. Seo, M. J. Lee, D. H. Seo, E. J. Jeoung, D.-S. Suh, Y. S. Joung, I. K. Yoo, I. R. Hwang, S. H. Kim, I. S. Byun, J.-S. Kim, J. S. Choi, and B. H. Park, Appl. Phys. Lett. **85,** 5655 (2004).
4. B. J. Choi, D. S. Jeong, S. K. Kim, C. Rohde, S. Choi, J. H. Oh, H. J. Kim, C. S. Hwang, K. Szot, R. Waser, B. Reichenberg, and S. Tiedke, J. Appl. Phys. **98,** 033715 (2005).
5. K. M. Kim, B. J. Choi, B. W. Koo, S. Choi, D. S. Jeong, and C. S. Hwang, Electrochem. Solid-State Lett. **9,** G343 (2006).
6. A. Chen, S. Haddad, Y.-C. Wu, T.-N. Fang, Z. Lan, S. Avanzino, S. Pangrle, M. Buynoski, M. Rathor, W. Cai, N. Tripsas, C. Bill, M. VanBuskirk, and M. Taguchi, in *Proceedings of 2005 IEDM Tech. Digest. Electron Devices Meeting* 746 (2005).
7. P. Zhou, M. Yin, H. J. Wan, H. B. Lu, T. A. Tang, and Y. Y. Lin, Appl. Phys. Lett. **94,** 053510 (2009).
8. D. Lee, H. Choi, H. Sim, D. Choi, H. Hwang, M.-J. Lee, S.-A. Seo, and I. K. Yoo, IEEE Electron. Device Lett. **26,** 719 (2005).
9. X. Wu, P. Zhou, J. Li, L. Y. Chen, H. B. Lv, Y. Y. Lin, and T. A. Tang, Appl. Phys. Lett. **90,** 183507 (2007).
10. W. Guan, S. Long, R. Jia, and M. Liu, Appl. Phys. Lett. **91,** 062111 (2007).
11. Q. Xiao, S. Shao, J. Shao, and Z. Fan, Chin. Opt. Lett. **7,** 162 (2009).
12. Q. Liu, W. Guan, S. Long, M. Liu, S. Zhang, Q. Wang, and J. Chen, J. Appl. Phys. **104,** 114514 (2008).
13. B. Sun, L.-F. Liu, D.-D. Han, Y. Wang, X.-Y. Liu, R.-Q. Han, and J.-F. Kang, Chin. Phys. Lett. **25,** 2187 (2008).
14. W. Guan, S. Long, Q. Liu, M. Liu, and W. Wang, IEEE Electron. Device Lett. **29,** 434 (2008).